# Multifunctional Fe$_3$O$_4$@Polydopamine Core–Shell Nanocomposites for Intracellular mRNA Detection and Imaging-Guided Photothermal Therapy

Li-Sen Lin,[†] Zhong-Xiao Cong,[†] Jian-Bo Cao,[‡] Kai-Mei Ke,[†] Qiao-Li Peng,[‡] Jinhao Gao,[‡] Huang-Hao Yang,[†,*] Gang Liu,[‡,*] and Xiaoyuan Chen[§]

[†]The Key Lab of Analysis and Detection Technology for Food Safety of the MOE, College of Chemistry, Fuzhou University, Fuzhou 350108, China, [‡]State Key Laboratory of Molecular Vaccinology and Molecular Diagnostics & Center for Molecular Imaging and Translational Medicine, School of Public Health, Xiamen University, Xiamen 361005, China, and [§]Laboratory of Molecular Imaging and Nanomedicine (LOMIN), National Institute of Biomedical Imaging and Bioengineering (NIBIB), National Institutes of Health (NIH), Bethesda, Maryland 20892, United States. The manuscript was written through contributions of all authors. All authors have given approval to the final version of the manuscript.

ABSTRACT Multifunctional nanocomposites have the potential to integrate sensing, diagnostic, and therapeutic functions into a single nanostructure. Herein, we synthesize Fe$_3$O$_4$@polydopamine core–shell nanocomposites (Fe$_3$O$_4$@PDA NCs) through an *in situ* self-polymerization method. Dopamine, a melanin-like mimic of mussel adhesive proteins, can self-polymerize to form surface-adherent polydopamine (PDA) films onto a wide range of materials including Fe$_3$O$_4$ nanoparticles used here. In such nanocomposites, PDA provides a number of advantages, such as near-infrared absorption, high fluorescence quenching efficiency, and a surface for further functionalization with biomolecules. We demonstrate the ability of the Fe$_3$O$_4$@PDA NCs to act as theranostic agents for intracellular mRNA detection and multimodal imaging-guided photothermal therapy. This work would stimulate interest in the use of PDA as a useful material to construct multifunctional nanocomposites for biomedical applications.
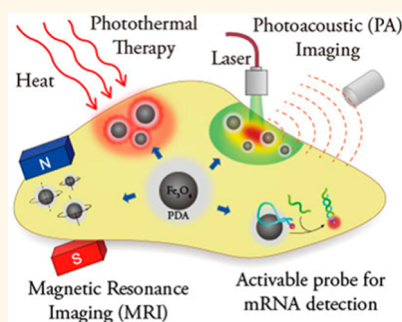
Recent advances in nanoscience and biomedicine have driven the development of multifunctional nanocomposites that combine sensing, diagnostic, and therapeutic functions within a single nanostructure.[1−10] Benefiting from the significantly improved physical, chemical, and biological properties, such multifunctional nanocomposites offer an opportunity for multimodal bioimaging and theranostic applications.[11−14] Lately, much effort has been devoted to the fabrication of multifunctional nanocomposites, such as graphene oxide-Fe$_3$O$_4$,[11] Fe$_3$O$_4$@Au,[12] and Fe$_3$O$_4$@Cu$_{2−x}$S.[13] Dopamine (DA), one of the most important neurotransmitters, is also a small-molecule mimic of the adhesive proteins of mussels. It can self-polymerize at alkaline pH values, and the generated polydopamine (PDA) can spontaneously deposit on virtually any surface to form a conformal layer.[15] Moreover, PDA is stable and biocompatible *in vivo*,[16]

which makes it a suitable material for biomedical applications. Furthermore, the existence of functional groups (*i.e.*, catechol and amine) on the surface of PDA enhances the binding of various biomolecules.[15,17−20] Very recently, PDA has been used as a photothermal therapeutic agent for *in vivo* cancer therapy because of its strong near-infrared (NIR) absorption and high photothermal conversion efficiency (40%).[21] Considering these features, we hypothesize that PDA could be a useful material in the preparation of multifunctional nanocomposites for theranostic applications.
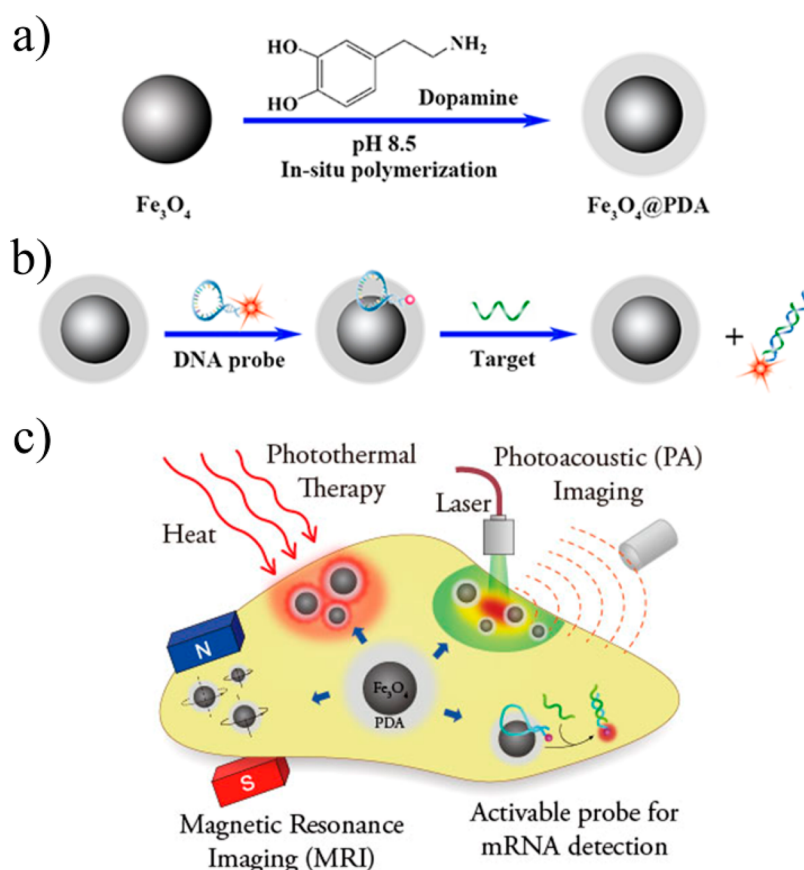
Messenger RNA (mRNA), a single-stranded ribonucleic acid, is also the blueprint for the cellular production of proteins. Moreover, some mRNAs are disease-relevant and can be utilized as markers to determine the stage of the disease.[22] Recently, several methods such as microarray analysis[23] and real-time

Figure 1. (a) Schematic illustration of the preparation of Fe_3O_4@PDA NCs. (b) RNA detection with the Fe_3O_4@PDA-based nanoprobe. (c) Application of Fe_3O_4@PDA NCs for intracellular mRNA detection and multimodal imaging-guided photothermal therapy.

polymerase chain reaction (RT-PCR)[24] have been developed for mRNA detection. Although these methods are effective for detecting mRNA expression in bulk samples, they are incapable of identifying cell-to-cell mutations. Significantly, many important biological processes not only are related with bulk mRNA expression, but also rely highly on cell-to-cell variations in mRNA.[25] Thus, it is necessary to develop useful approaches for detecting mRNA in living cells.[26−32]

In this work, we fabricated multifunctional Fe_3O_4@ polydopamine core−shell nanocomposites (Fe_3O_4@PDA NCs) consisting of a Fe_3O_4 core surrounded by a thin PDA shell, which can be utilized for intracellular mRNA detection and multimodal imaging-guided photothermal therapy (PTT). Although the synthesis of Fe_3O_4@PDA NCs has been reported,[33,34] to the best of our knowledge, the theranostic applications of Fe_3O_4@PDA NCs have not been explored until now. The modification of the Fe_3O_4 nanoparticles (Fe_3O_4 NPs) with PDA was achieved by *in situ* polymerization of DA onto the surface of the Fe_3O_4 NPs (Figure 1a). Furthermore, we demonstrated that PDA can adsorb dye-labeled single-stranded DNA (ssDNA) probe and effectively quench the fluorescence of the dye. In the presence of the target, the specific binding between the dye-labeled ssDNA probe and its target induces the formation of a duplex structure, resulting in

the release of the probe from PDA and subsequent recovery of the fluorescence (Figure 1b). Therefore, the Fe_3O_4@PDA NCs could be used to design a nanoprobe for the detection of mRNA in living cells. Moreover, the Fe_3O_4 core enhances the capacity of Fe_3O_4@PDA NCs as contrast agents for magnetic resonance imaging (MRI), which could be used to monitor the delivery of the DNA probe and guide therapy. In addition, due to the NIR absorption of the PDA, Fe_3O_4@PDA NCs can be employed for photoacoustic (PA) imaging and PTT (Figure 1c). Our results suggest a high potential for the use of PDA in the construction of multifunctional nanocomposites for simultaneous diagnosis and therapy of cancer.

RESULTS AND DISCUSSION

Fe_3O_4 NPs were easily coated with a uniform PDA shell by dispersing them in an alkaline DA solution and mildly shaking at room temperature for 4 h. Transmission electron microscopy (TEM) revealed that approximately a 4 nm thick PDA shell was wrapped on the surface of the Fe_3O_4 NPs after self-polymerization of the DA (Figure 2a). The dynamic light scattering (DLS) data showed that the hydrodynamic diameter of the Fe_3O_4 NPs was increased after the PDA coating (Supporting Information Figure S1), which is consistent with the TEM results. Moreover, the Fe_3O_4@PDA NCs
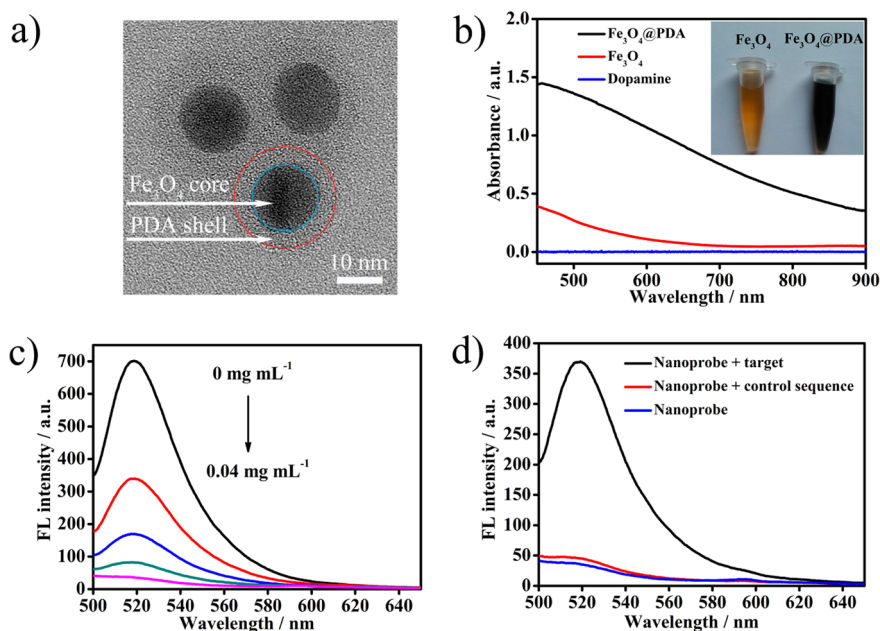
Figure 2. (a) TEM image of the Fe_3O_4@PDA NCs obtained by self-polymerization of DA on the surface of Fe_3O_4 NPs. (b) UV−vis absorption spectra of Fe_3O_4 NPs (0.1 mg mL^{-1}) before and after PDA coating. The inset photo shows the color change between Fe_3O_4 NPs and Fe_3O_4@PDA NCs. (c) Fluorescence quenching of 50 nM FAM-hpDNA in the presence of Fe_3O_4@PDA NCs with a series of concentrations (0, 0.01, 0.02, 0.03, 0.04 mg mL^{-1}). (d) Fluorescence emission spectra of Fe_3O_4@PDA-DNA nanoprobe treated with 200 nM complementary target and 200 nM noncomplementary control sequence. Excitation: 480 nm, emission: 520 nm.

exhibited excellent stability in physiological solutions including serum (Supporting Information Figure S2a). The Fe_3O_4:PDA weight ratio in the Fe_3O_4@PDA NCs was measured to be 1:0.8 as determined by inductive coupling plasma (ICP) measurement of Fe content. In addition, the thickness of the PDA shell was decreased to about 1.5 nm by reducing the polymerization time to 1 h (Supporting Information Figure S2b−d). Moreover, compared to the Fe_3O_4 NPs, Fe_3O_4@PDA NCs displayed a remarkably higher NIR absorption, which was contributed by the PDA layer and is favorable for photothermal therapy (Figure 2b).

PDA has numerous functional groups such as amino and catechol, which can facilitate the further functionalization of PDA-based nanocomposites with biomolecules. The adsorption and fluorescence quenching abilities of the Fe_3O_4@PDA NCs toward the dye-labeled ssDNA were evaluated *via* measurements made while mixing the fluorescent DNA probe and the prepared Fe_3O_4@PDA NCs. Since hairpin ssDNA (hpDNA) can provide increased target recognition specificity than the linear ssDNA, we chose a FAM-labeled hairpin ssDNA (FAM-hpDNA) containing a 21-base single-stranded loop and a 6-base-pair stem as the recognition probe (all sequences are shown in the Supporting Information Table S1). As shown in Figure 2c, the fluorescence of the FAM-hpDNA was almost entirely quenched in the presence of 0.04 mg mL^{-1} of Fe_3O_4@PDA NCs, indicating the strong adsorption of the hpDNA onto the Fe_3O_4@PDA NCs and the high fluorescence quenching efficiency of the Fe_3O_4@PDA

NCs. In contrast, the fluorescence did not change significantly with the addition of Fe_3O_4 NPs (Supporting Information Figure S3). Given that PDA contains catechol groups, the binding of the ssDNA to the Fe_3O_4@PDA NCs is likely due to $\pi-\pi$ stacking interactions between the nucleobases and aromatic groups of the PDA. Moreover, PDA displayed a quenching efficiency of up to 95%, which is comparable to that of gold nanoparticles[27] and graphene oxide.[29] The performance of the Fe_3O_4@PDA-DNA nanoprobe prepared by mixing FAM-hpDNA with Fe_3O_4@PDA NCs was first evaluated in a buffer system. As shown in Figure 2d, the nanoprobe responded with a 9.5-fold increase in the fluorescence signal upon the addition of 200 nM of the complementary target. In contrast, the fluorescence signal did not obviously change in the presence of a noncomplementary sequence and was of a magnitude comparable to the background fluorescence. In addition, the fluorescence intensity of the nanoprobe increased with increasing concentration of the RNA target from 0 to 200 nM (Supporting Information Figure S4). These results demonstrated that the Fe_3O_4@PDA-based nanoprobe can effectively signal the presence of a specific target. Moreover, the Fe_3O_4@PDA-DNA nanoprobe was stable in serum (Supporting Information Figure S5).

After testing the signaling ability of the Fe_3O_4@PDA-DNA nanoprobe with a synthetic target, their ability to detect intracellular mRNA was further investigated with a normal immortalized human mammary epithelial cell line (MCF-10A), in which the c-myc mRNA

a)

b)
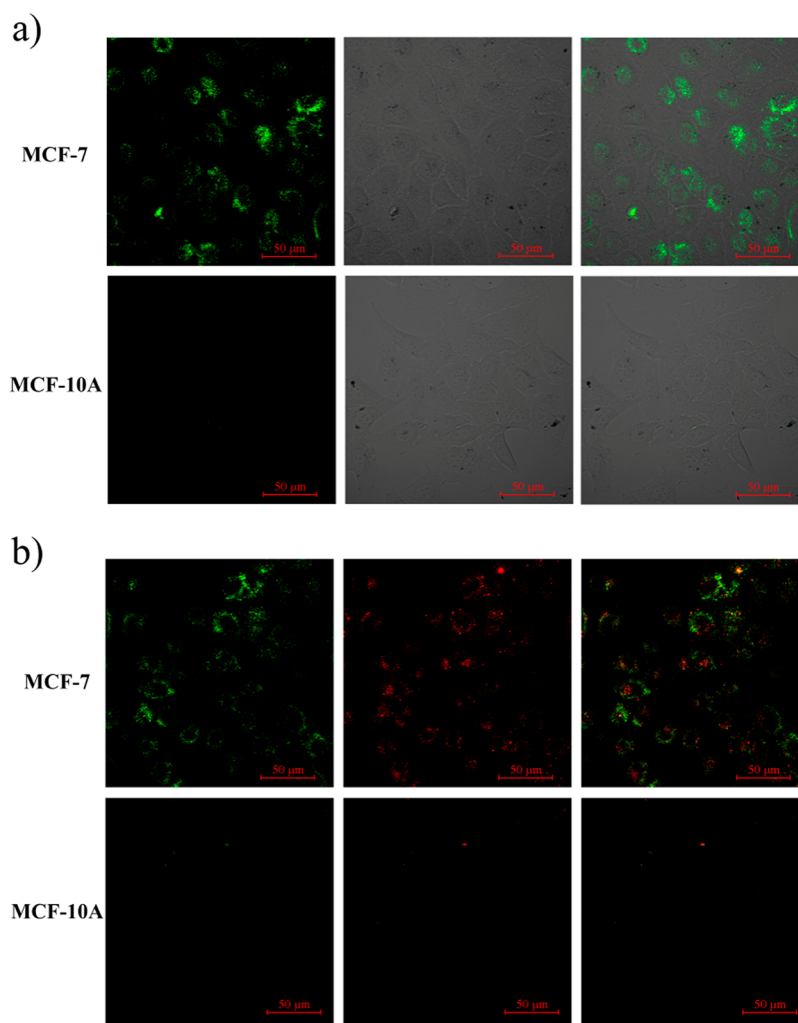
Figure 3. (a) Intracellular testing of the Fe$_3$O$_4$@PDA-based nanoprobe. CLSM images of MCF-7 and MCF-10A cells treated with the nanoprobe. Left panels are FAM fluorescence associated with c-myc mRNA, center panels are bright field image of cells, and right panels are the overlay of FAM fluorescence and the bright field image. (b) Simultaneous detection of multiple mRNAs in living cells. CLSM images of MCF-7 and MCF-10A cells treated with multiplexed nanoprobes. Left panels are FAM fluorescence associated with c-myc mRNA, center panels are Cy3 fluorescence associated with TK1 mRNA, and right panels are the overlay of FAM fluorescence and Cy3 fluorescence. Scale bars are 50 μm.

is expressed normally, and a human breast cancer cell line (MCF-7), in which the c-myc mRNA is overexpressed.[35] C-myc is a potent activator of tumorigenesis and is dysregulated in a range of cancers. The loop region of the FAM-hpDNA was designed to be complementary to c-myc mRNA. Confocal laser scanning microscopy (CLSM) results showed that the MCF-7 cells treated with the Fe$_3$O$_4$@PDA-DNA nanoprobe displayed a strong green fluorescence (Figure 3a). In comparison, the fluorescence of the MCF-10A cells incubated with the nanoprobe under the same conditions was very low. These results demonstrated that the Fe$_3$O$_4$@PDA-based nanoprobe is useful for detecting intracellular mRNA.

Importantly, cancer is often related with multiple specific mRNAs. The simultaneous detection of multiple mRNA targets is useful for increasing the accuracy of early diagnosis of cancer.[26] Moreover, the Fe$_3$O$_4$@PDA NCs exhibited a broad absorption range of 450–900 nm, which makes them potential energy

acceptors and quenchers for a variety of fluorescence dyes. Thus, we hypothesized that the Fe$_3$O$_4$@PDA NCs could be exploited to design multiplexed nanoprobes for simultaneous detection of multiple mRNAs. Thymidine kinase 1 (TK1) mRNA, an important marker of tumor growth, is also overexpressed in MCF-7 cells.[36] A Cy3-labled hairpin ssDNA (Cy3-hpDNA) targeting TK1 mRNA was used as the second recognition probe. After adding two DNA recognition probes (FAM-hp DNA and Cy3-hpDNA) to the Fe$_3$O$_4$@PDA NCs and mixing for 10 min, the as-prepared multiplexed nanoprobes were used to detect multiple mRNAs simultaneously in living cells. As shown in Figure 3b, after incubation with the multiplexed nanoprobes, both the green fluorescence (c-myc mRNA) and red fluorescence (TK1 mRNA) were much stronger in the MCF-7 cells than those in the MCF-10A cells. These results showed that Fe$_3$O$_4$@PDA-based multiplexed nanoprobes can be used to detect multiple mRNAs in living cells. In addition, the
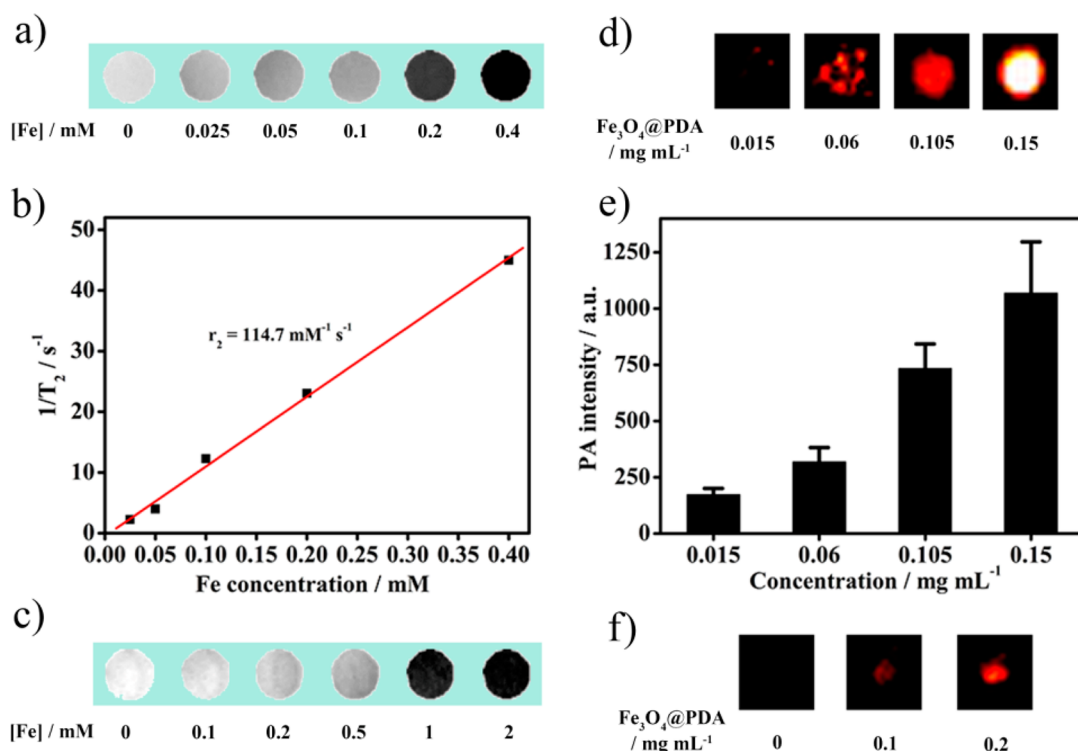
Figure 4. (a) T_2-weighted MR images of the Fe_3O_4@PDA NCs in aqueous solution at different Fe concentrations. (b) Corresponding T_2 relaxation rate of the Fe_3O_4@PDA NCs as a function of Fe concentration. (c) T_2-weighted MR images of MCF-7 cells (5×10^5) incubated with the Fe_3O_4@PDA NCs at different Fe concentrations. (d) PA images and (e) corresponding PA intensity of the Fe_3O_4@PDA NCs with different concentrations. (f) PA images of MCF-7 cells (5×10^5) incubated with different concentrations of Fe_3O_4@PDA NCs.

Fe_3O_4@PDA-based nanoprobe also could distinguish cancer cells from normal cells based on the different mRNA expression levels.

As a noninvasive imaging technique with high spatial resolution, MRI is a powerful tool for early detection of cancer and therapeutic response assessment. Magnetic nanoparticles have been widely used as contrast agents for MRI. Nowadays, two superparamagnetic iron oxide (SPIO) agents are clinically approved, and newer SPIOs with clinically relevant characteristics remain to be further developed. In this work, Fe_3O_4@PDA NCs aqueous solutions at different Fe concentrations were investigated by T_2-weighted MRI on a 9.4 T small animal MR scanner in order to evaluate their contrast enhancement effect. As shown in Figure 4a, the T_2 signal intensity decreased significantly with increasing Fe concentration, because of the dipolar interaction of the magnetic moments of the Fe_3O_4@PDA NCs with protons in the water.[37] In addition, the T_2 relaxation rate ($r_2 = 1/T_2$) of the Fe_3O_4@PDA NCs was calculated to be 114.7 $mM^{-1} s^{-1}$ (Figure 4b). We next used Fe_3O_4@PDA NCs for MR imaging of cancer cells (Figure 4c). The MCF-7 cells treated with the Fe_3O_4@PDA NCs showed significantly reduced signal intensity in the T_2-weighted MR images in comparison to the untreated cells. Moreover, the dark intensity of their T_2-weighted images increased in an Fe concentration-dependent manner. These results indicated that the Fe_3O_4@PDA NCs

could be used as promising contrast agents for MRI applications.

PA imaging is a novel imaging technique that combines the advantages of optical and ultrasound imaging.[38,39] The use of an NIR light in PA imaging greatly enhances the penetration depth.[40] The NIR absorption of PDA motivated us to study the PA property of the Fe_3O_4@PDA NCs. As shown in Figure 4d,e, the PA signal increased with the increasing concentration of Fe_3O_4@PDA NCs at 760 nm, suggesting that the Fe_3O_4@PDA NCs would be good candidates for PA imaging of cancer cells. As expected, a much stronger PA signal was observed in the MCF-7 cells incubated with the Fe_3O_4@PDA NCs as compared to the control cells incubated without the Fe_3O_4@PDA NCs (Figure 4f). These results demonstrated the great potential of the Fe_3O_4@PDA NCs for PA imaging.

An important feature of Fe_3O_4@PDA NCs is their NIR light-induced thermal effect, which could be used for photothermal therapy. To study the photothermal effect induced by NIR irradiation, different concentrations of Fe_3O_4@PDA NCs were irradiated by an NIR laser (808 nm, 1 W cm^{-2}) for 10 min. The temperatures of these Fe_3O_4@PDA NCs solutions increased with the irradiation time, and the temperature increased more rapidly as the concentration of the Fe_3O_4@PDA NCs was increased (Figure 5a). Moreover, the temperature of the Fe_3O_4@PDA NCs solution at a concentration of
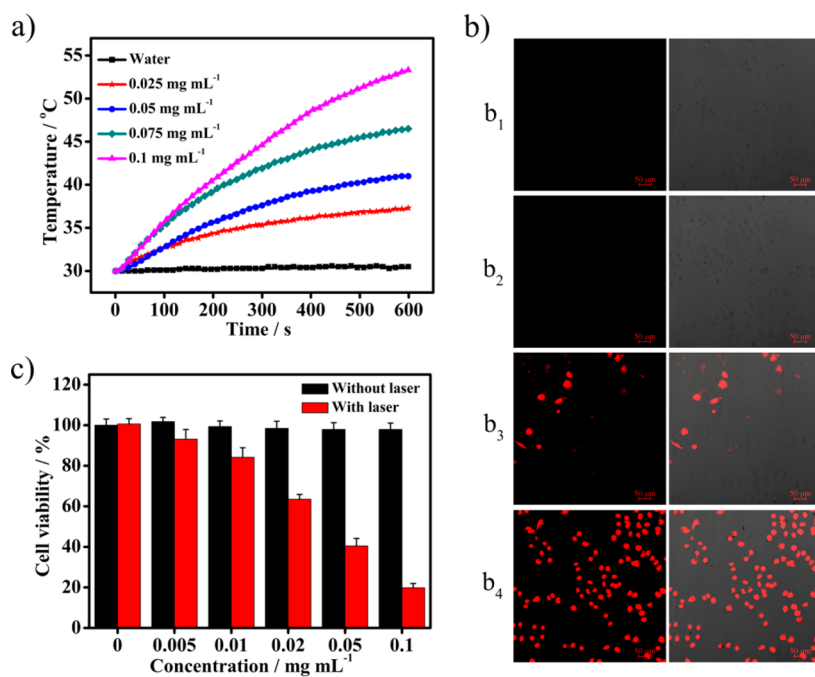
Figure 5. (a) Temperature elevation of different concentrations of Fe$_3$O$_4$@PDA NCs as a function of irradiation time. (b) CLSM images of differently treated MCF-7 cells stained with PI: (b$_1$) 5 min of laser irradiation only; (b$_2$) Fe$_3$O$_4$@PDA NCs only; (b$_3$) Fe$_3$O$_4$@PDA NCs and 2 min of laser irradiation; and (b$_4$) Fe$_3$O$_4$@PDA NCs and 5 min of laser irradiation. Left panels are PI fluorescence corresponding to dead cells, and right panels are the overlay of PI fluorescence and the bright field image. Scale bars are 50 μm. (c) Cell viability of MCF-7 cells exposed to different concentrations of Fe$_3$O$_4$@PDA NCs with or without laser irradiation.

0.1 mg mL^{-1} was raised from 29.5 to 53.3 °C after irradiation for 10 min. In comparison, the temperature of pure water was increased by only 0.6 °C under the same laser exposure condition. It has been reported that cancer cells can be killed after being kept at 42 °C for 15−60 min, and the duration can be shortened to 4−6 min when the temperatures is over 50 °C.[41] This photothermal effect implied that the Fe$_3$O$_4$@PDA NCs would be effective photothermal agents for cancer therapy. To verify this, the MCF-7 cells were incubated with 0.1 mg mL^{-1} of Fe$_3$O$_4$@PDA NCs for 4 h and were then irradiated by an 808 nm laser at a power density of 2 W cm^{-2} for 5 min. After the treatment, the cells were stained with propidium iodide (PI), which only incorporates into dead cells. The CLSM results showed that the Fe$_3$O$_4$@PDA NCs could effectively kill the cancer cells only through the photothermal effect induced by the NIR irradiation, while neither the Fe$_3$O$_4$@PDA NCs nor the laser irradiation alone can lead to cell death (Figure 5b). In addition, cells treated with Fe$_3$O$_4$ NPs and irradiated by NIR laser under the same condition showed negligible cell death (Supporting Information Figure S6). The photothermal cytotoxicity of Fe$_3$O$_4$@PDA NCs on cancer cells was further quantitatively evaluated using an MTT assay. As shown in Figure 5c, MCF-7 cells treated with the Fe$_3$O$_4$@PDA NCs without laser irradiation remained more than 95% viable at concentrations up to 0.1 mg mL^{-1}. In contrast, the cell viability significantly decreased when the MCF-7 cells were exposed to Fe$_3$O$_4$@PDA NCs and irradiated with

the NIR laser. Furthermore, no apparent loss of cell viability was observed when cells were incubated with the Fe$_3$O$_4$@PDA NCs at a concentration as high as 0.4 mg mL^{-1} for 24 h (Supporting Information Figure S7), indicating the excellent biocompatibility and low toxicity of the Fe$_3$O$_4$@PDA NCs. These results indicated that the combination of Fe$_3$O$_4$@PDA NCs and NIR laser irradiation can kill the cancer cells effectively, and thus the highly biocompatible Fe$_3$O$_4$@PDA NCs can act as NIR-absorbing agents for photothermal therapy of cancer.

CONCLUSIONS

In summary, we have synthesized Fe$_3$O$_4$@PDA NCs as multifunctional theranostic agents for intracellular mRNA detection and multimodal imaging-guided photothermal therapy. On the one hand, the PDA can adsorb dye-labeled ssDNA probes, while on the other hand, the PDA possesses a high fluorescence quenching efficiency. Therefore, the Fe$_3$O$_4$@PDA NCs can be used to construct nanoprobes for the detection of mRNA in living cells. Moreover, because of the magnetism of the Fe$_3$O$_4$ core and the NIR absorption of the PDA, the Fe$_3$O$_4$@PDA NCs can be employed for MRI and PA imaging, which would also be useful for monitoring the delivery of DNA probes and guiding therapy. Furthermore, the Fe$_3$O$_4$@PDA NCs can kill cancer cells effectively with the use of an NIR laser. Overall, the use of PDA for the construction of multifunctional nanocomposites has several significant advantages,

including the following: (1) the PDA can be easily obtained by the self-polymerization of DA, and it spontaneously adheres to virtually any surface; (2) PDA is hydrophilic and biocompatible, which are essential traits for biomedical applications; (3) PDA possesses a high fluorescence quenching ability, which can be used to design nanosensors for the detection of biomolecules; (4) the NIR absorption of PDA makes the PDA-based nanocomposites promising agents for PA imaging and PTT; and (5) PDA can react with thiol- and amino-terminated molecules *via* the Michael addition or Schiff base reactions,[15,17−20] which can facilitate the surface functionalization of the nanocomposites with biomolecules for targeting specific cells. Thus, we anticipate that the mussel-inspired PDA will be highly useful in the design of novel multifunctional nanocomposites for biomedical applications.

MATERIALS AND METHODS

Materials. Water-soluble iron oxide (Fe_3O_4) nanoparticles with carboxylic acid group (*ca.* 15 nm) were obtained from Ocean NanoTech (Springdale, AR, USA). Dopamine hydrochloride and 3-(4,5-dimethyl-thiazol-2-yl)-2,5-diphenyltetrazolium bromide (MTT) were purchased from Sigma (St. Louis, MO, USA). DNA and RNA sequences were synthesized and purified by Sangon Biotechnology Co., Ltd. (Shanghai, China) and TaKaRa Biotechnology Co., Ltd. (Dalian, China). All chemicals were used without further purification, and Milli-Q water was used throughout this study.

Synthesis of Fe_3O_4@PDA NCs. In a typical synthesis of Fe_3O_4@PDA NCs with 4 nm thickness of PDA shell, 6 mg of dopamine was added to 50 mL of 10 mM PBS (pH 8.5) containing 5 mg of Fe_3O_4 NPs. After shaking at room temperature for 4 h, Fe_3O_4@PDA NCs were obtained by centrifugation and washed with water for three times.

Preparation of Fe_3O_4@PDA-DNA Nanoprobe. 500 nM FAM-hpDNA was added to 0.4 mg mL^{-1} of Fe_3O_4@PDA NCs. After mixing for 10 min, the as-prepared Fe_3O_4@PDA-DNA nanoprobe was stored at 4 °C for further use. The multiplexed nanoprobe was prepared by means of the similar procedure.

Fluorescence Response of Fe_3O_4@PDA-Based Nanoprobe to Target in Buffer. 0.04 mg mL^{-1} of Fe_3O_4@PDA-DNA nanoprobe (containing 50 nM FAM-hpDNA) was mixed with different concentrations of target RNA (0, 2, 5, 10, 20, 50, 100, and 200 nM) for 1 h, and then the fluorescence spectra of all samples were recorded with a Hitachi F-4600 fluorescence spectrophotometer (Hitachi Co., Ltd., Japan). Noncomplementary sequence (200 nM) was used as a negative control to verify the specific binding of the nanoprobe and the target RNA.

Confocal Fluorescence Imaging. In comparative experiment of cancer cells and normal cells, MCF-7 cells and MCF-10A cells were seeded in 35-mm confocal dish for 24 h. Then cells were washed three times with PBS and incubated with Fe_3O_4@PDA-DNA nanoprobe at 37 °C for 12 h. Subsequently, confocal imaging was performed on a Nikon C2 confocal microscope (Nikon, Tokyo, Japan) with a 60× oil-immersion objective.

Magnetic Resonance Imaging. MCF-7 cells seeded in 6-well plates (5 × 10^5 cells/well) were incubated with Fe_3O_4@PDA NCs at different Fe concentrations (0, 0.1, 0.2, 0.5, 1, and 2 mM) for 12 h. The cells were then washed with PBS and harvested before MRI.

Photoacoustic Imaging. MCF-7 cells (5 × 10^5) were incubated with different concentrations of Fe_3O_4@PDA NCs at 37 °C for 12 h. Then, the cells were washed three times with PBS and harvested by trypsinization. After being transferred to a 0.2 mL microtube and centrifuged, the photoacoustic images of cell pellets were obtained at 760 nm using a PA system (Endra Nexus 128, Ann Arbor, MI).

Cytotoxicity Assay. The *in vitro* cytotoxicity was measured using a standard MTT assay. MCF-7, HeLa, and HepG2 cells were seeded into 96-well cell-culture plate at 1.5 × 10^4 cells/well and then incubated for 24 h at 37 °C under 5% CO_2. After incubating the cells with various concentrations of Fe_3O_4@PDA NCs for another 24 h, the standard MTT assay was carried out to determine the cell viabilities relative to the control untreated cells.

Measurement of Photothermal Performance. Fe_3O_4@PDA NCs with different concentrations (0−0.1 mg mL^{-1}) were suspended in quartz cuvette (total volume of 1 mL) and irradiated by a NIR laser at 808 nm (BWT Beijing LTD, China) with output power of 1 W cm^{-2} for 10 min. The temperature of the solutions was measured by a digital thermometer with a thermocouple probe.

Photothermal Therapy. MCF-7 cells seeded in 35-mm confocal dish were incubated with 0.1 mg mL^{-1} of Fe_3O_4 NPs or Fe_3O_4@PDA NCs for 4 h. After exposure to NIR laser (808 nm, 2 W cm^{-2}) for certain time, the cells were stained with propidium iodide and imaged by confocal laser scanning microscopy.

To quantitatively evaluate the photothermal cytotoxicity of Fe_3O_4@PDA NCs, MCF-7 cells were incubated in 96-well plates at 37 °C in a humidified atmosphere containing 5% CO_2 for 24 h. The Fe_3O_4@PDA NCs with different concentrations were added, and the cells were further incubated for 4 h. After exposure to NIR laser (808 nm, 2 W cm^{-2}) for 5 min, the cells were allowed to incubate for another 24 h. The standard MTT assay was carried out to evaluate the cell viability.

Conflict of Interest: The authors declare no competing financial interest.

REFERENCES AND NOTES

1. Lee, J. E.; Lee, N.; Kim, T.; Kim, J.; Hyeon, T. Multifunctional Mesoporous Silica Nanocomposite Nanoparticles for Theranostic Applications. *Acc. Chem. Res.* **2011**, *44*, 893–902.

2. Lee, D.-E.; Koo, H.; Sun, I.-C.; Ryu, J. H.; Kim, K.; Kwon, I. C. Multifunctional Nanoparticles for Multimodal Imaging and Theragnosis. *Chem. Soc. Rev.* **2012**, *41*, 2656–2672.

3. Gao, J.; Gu, H.; Xu, B. Multifunctional Magnetic Nanoparticles: Design, Synthesis, and Biomedical Applications. *Acc. Chem. Res.* **2009**, *42*, 1097–1107.

4. Jin, Y.; Jia, C.; Huang, S.-W.; O'Donnell, M.; Gao, X. Multifunctional Nanoparticles as Coupled Contrast Agents. *Nat. Commun.* **2010**, *1*, 41.

5. Hu, S.-H.; Gao, X. Nanocomposites with Spatially Separated Functionalities for Combined Imaging and Magnetolytic Therapy. *J. Am. Chem. Soc.* **2010**, *132*, 7234–7237.

6. Xiao, Z.; Levy-Nissenbaum, E.; Alexis, F.; Lupták, A.; Teply, B. A.; Chan, J. M.; Shi, J.; Digga, E.; Cheng, J.; Langer, R.; *et al.* Engineering of Targeted Nanoparticles for Cancer Therapy Using Internalizing Aptamers Isolated by Cell-Uptake Selection. *ACS Nano* **2012**, *6*, 696–704.

7. Kim, D.; Jeong, Y. Y.; Jon, S. A Drug-Loaded Aptamer-Gold Nanoparticle Bioconjugate for Combined CT Imaging and Therapy of Prostate Cancer. *ACS Nano* **2010**, *4*, 3689–3696.

8. Schladt, T. D.; Shukoor, M. I.; Schneider, K.; Tahir, M. N.; Natalio, F.; Ament, I.; Becker, J.; Jochum, F. D.; Weber, S.; Köhler, O.; *et al.* Au@MnO Nanoflowers: Hybrid Nanocomposites for Selective Dual Functionalization and Imaging. *Angew. Chem., Int. Ed.* **2010**, *49*, 3976–3980.

9. Wang, J.; Zhu, G.; You, M.; Song, E.; Shukoor, M. I.; Zhang, K.; Altman, M. B.; Chen, Y.; Zhu, Z.; Huang, C. Z.; *et al.* Assembly of Aptamer Switch Probes and Photosensitizer on Gold Nanorods for Targeted Photothermal and Photodynamic Cancer Therapy. *ACS Nano* **2012**, *6*, 5070–5077.

10. Lovell, J. F.; Jin, C. S.; Huynh, E.; Jin, H.; Kim, C.; Rubinstein, J. L.; Chan, W. C. W.; Cao, W.; Wang, L. V.; Zheng, G. Porphysome Nanovesicles Generated by Porphyrin Bilayers for Use as Multimodal Biophotonic Contrast Agents. *Nat. Mater.* **2011**, *10*, 324–332.

11. Yang, K.; Hu, L.; Ma, X.; Ye, S.; Cheng, L.; Shi, X.; Li, C.; Li, Y.; Liu, Z. Multimodal Imaging Guided Photothermal Therapy Using Functionalized Graphene Nanosheets Anchored with Magnetic Nanoparticles. *Adv. Mater.* **2012**, *24*, 1868–1872.

12. Dong, W.; Li, Y.; Niu, D.; Ma, Z.; Gu, J.; Chen, Y.; Zhao, W.; Liu, X.; Liu, C.; Shi, J. Facile Synthesis of Monodisperse Super-paramagnetic Fe_3O_4 Core@hybrid@Au Shell Nanocomposite for Bimodal Imaging and Photothermal Therapy. *Adv. Mater.* **2011**, *23*, 5392–5397.

13. Tian, Q.; Hu, J.; Zhu, Y.; Zou, R.; Chen, Z.; Yang, S.; Li, R.; Su, Q.; Han, Y.; Liu, X. Sub-10 nm $Fe_3O_4@Cu_{2−x}S$ Core-Shell Nanoparticles for Dual-Modal Imaging and Photothermal Therapy. *J. Am. Chem. Soc.* **2013**, *135*, 8571–8577.

14. Wang, C.; Xu, H.; Liang, C.; Liu, Y.; Li, Z.; Yang, G.; Cheng, L.; Li, Y.; Liu, Z. Iron Oxide @ Polypyrrole Nanoparticles as a Multifunctional Drug Carrier for Remotely Controlled Cancer Therapy with Synergistic Antitumor Effect. *ACS Nano* **2013**, *7*, 6782–6795.

15. Lee, H.; Dellatore, S. M.; Miller, W. M.; Messersmith, P. B. Mussel-Inspired Surface Chemistry for Multifunctional Coatings. *Science* **2007**, *318*, 426–430.

16. Liu, X.; Cao, J.; Li, H.; Li, J.; Jin, Q.; Ren, K.; Ji, J. Mussel-Inspired Polydopamine: A Biocompatible and Ultrastable Coating for Nanoparticles *In Vivo*. *ACS Nano* **2013**, *7*, 9384–9395.

17. Lee, H.; Rho, J.; Messersmith, P. B. Facile Conjugation of Biomolecules onto Surfaces *via* Mussel Adhesive Protein Inspired Coatings. *Adv. Mater.* **2009**, *21*, 431–434.

18. Xu, L. Q.; Yang, W. J.; Neoh, K.-G.; Kang, E.-T.; Fu, G. D. Dopamine-Induced Reduction and Functionalization of Graphene Oxide Nanosheets. *Macromolecules* **2010**, *43*, 8336–8339.

19. Yang, S. H.; Kang, S. M.; Lee, K.-B.; Chung, T. D.; Lee, H.; Choi, I. S. Mussel-Inspired Encapsulation and Functionalization of Individual Yeast Cells. *J. Am. Chem. Soc.* **2011**, *133*, 2795–2797.

20. Ham, H. O.; Liu, Z.; Lau, K. H. A.; Lee, H.; Messersmith, P. B. Facile DNA Immobilization on Surfaces through a Catecholamine Polymer. *Angew. Chem., Int. Ed.* **2011**, *50*, 732–736.

21. Liu, Y.; Ai, K.; Liu, J.; Deng, M.; He, Y.; Lu, L. Dopamine-Melanin Colloidal Nanospheres: An Efficient Near-Infrared Photothermal Therapeutic Agent for *In Vivo* Cancer Therapy. *Adv. Mater.* **2013**, *25*, 1353–1359.

22. Chen, T.; Wu, C. S.; Jimenez, E.; Zhu, Z.; Dajac, J. G.; You, M.; Han, D.; Zhang, X.; Tan, W. DNA Micelle Flares for Intracellular mRNA Imaging and Gene Therapy. *Angew. Chem., Int. Ed.* **2013**, *52*, 2012–2016.

23. Brown, P. O.; Botstein, D. Exploring the New World of the Genome with DNA Microarrays. *Nat. Genet.* **1999**, *21*, 33–37.

24. Nolan, T.; Hands, R. E.; Bustin, S. A. Quantification of mRNA Using Real-Time RT-PCR. *Nat. Protoc.* **2006**, *1*, 1559–1582.

25. Visvader, J. E. Cells of Origin in Cancer. *Nature* **2011**, *469*, 314–322.

26. Li, N.; Chang, C.; Pan, W.; Tang, B. A Multicolor Nanoprobe for Detection and Imaging of Tumor-Related mRNAs in Living Cells. *Angew. Chem., Int. Ed.* **2012**, *51*, 7426–7430.

27. Seferos, D. S.; Giljohann, D. A.; Hill, H. D.; Prigodich, A. E.; Mirkin, C. A. Nano-Flares: Probes for Transfection and mRNA Detection in Living Cells. *J. Am. Chem. Soc.* **2007**, *129*, 15477–15479.

28. Prigodich, A. E.; Seferos, D. S.; Massich, M. D.; Giljohann, D. A.; Lane, B. C.; Mirkin, C. A. Nano-flares for mRNA Regulation and Detection. *ACS Nano* **2009**, *3*, 2147–2152.

29. Ryoo, S.-R.; Lee, J.; Yeo, J.; Na, H.-K.; Kim, Y.-K.; Jang, H.; Lee, J. H.; Han, S. W.; Lee, Y.; Kim, V. N.; *et al.* Quantitative and Multiplexed MicroRNA Sensing in Living Cells Based on Peptide Nucleic Acid and Nano Graphene Oxide (PANGO). *ACS Nano* **2013**, *7*, 5882–5891.

30. Yang, R.; Jin, J.; Chen, Y.; Shao, N.; Kang, H.; Xiao, Z.; Tang, Z.; Wu, Y.; Zhu, Z.; Tan, W. Carbon Nanotube-Quenched Fluorescent Oligonucleotides: Probes that Fluoresce upon Hybridization. *J. Am. Chem. Soc.* **2008**, *130*, 8351–8358.

31. Su, S.; Wei, X.; Zhong, Y.; Guo, Y.; Su, Y.; Huang, Q.; Lee, S.-T.; Fan, C.; He, Y. Silicon Nanowire-Based Molecular Beacons for High-Sensitivity and Sequence-Specific DNA Multiplexed Analysis. *ACS Nano* **2012**, *6*, 2582–2590.

32. Lu, C.-H.; Zhu, C.-L.; Li, J.; Liu, J.-J.; Chen, X.; Yang, H.-H. Using Graphene to Protect DNA from Cleavage during Cellular Delivery. *Chem. Commun.* **2010**, *46*, 3116–3118.

33. Ma, Y.-R.; Zhang, X.-L.; Zeng, T.; Cao, D.; Zhou, Z.; Li, W.-H.; Niu, H.; Cai, Y.-Q. Polydopamine-Coated Magnetic Nanoparticles for Enrichment and Direct Detection of Small Molecule Pollutants Coupled with MALDI-TOF-MS. *ACS Appl. Mater. Interfaces* **2013**, *5*, 1024–1030.

34. Martín, M.; Salazar, P.; Villalonga, R.; Campuzano, S.; Pingarrón, J. M.; González-Mora, J. L. Preparation of Core-Shell Fe_3O_4@Poly(dopamine) Magnetic Nanoparticles for Biosensor Construction. *J. Mater. Chem. B* **2014**, *2*, 739–746.

35. Liao, D. J.; Dickson, R. B. C-myc in Breast Cancer. *Endocr.-Relat. Cancer* **2000**, *7*, 143–164.

36. Chen, C.-C.; Chang, T.-W.; Chen, F.-M.; Hou, M.-F.; Hung, S.-Y.; Chong, I.-W.; Lee, S.-C.; Zhou, T.-H.; Lin, S.-R. Combination of Multiple mRNA Markers (PTTG1, Survivin, UbcH10 and TK1) in the Diagnosis of Taiwanese Patients with Breast Cancer by Membrane Array. *Oncology* **2006**, *70*, 438–446.

37. Huang, J.; Bu, L.; Xie, J.; Chen, K.; Cheng, Z.; Li, X.; Chen, X. Effects of Nanoparticle Size on Cellular Uptake and Liver MRI with Polyvinylpyrrolidone-Coated Iron Oxide Nanoparticles. *ACS Nano* **2010**, *4*, 7151–7160.

38. Wang, L. V.; Hu, S. Photoacoustic Tomography: *In Vivo* Imaging from Organelles to Organs. *Science* **2012**, *335*, 1458–1462.

39. Dragulescu-Andrasi, A.; Kothapalli, S.-R.; Tikhomirov, G. A.; Rao, J.; Gambhir, S. S. Activatable Oligomerizable Imaging Agents for Photoacoustic Imaging of Furin-Like Activity in Living Subjects. *J. Am. Chem. Soc.* **2013**, *135*, 11015–11022.

40. Kim, C.; Favazza, C.; Wang, L. V. *In Vivo* Photoacoustic Tomography of Chemicals: High-Resolution Functional and Molecular Optical Imaging at New Depths. *Chem. Rev.* **2010**, *110*, 2756–2782.

41. Habash, R. W. Y.; Bansal, R.; Krewski, D.; Alhafid, H. T. Thermal Therapy, Part 1: An Introduction to Thermal Therapy. *Crit. Rev. Biomed. Eng.* **2006**, *34*, 459–489.